JACS Au
AN OPEN ACCESS JOURNAL OF THE AMERICAN CHEMICAL SOCIETY

pubs.acs.org/jacsau Article

Di- and Tetrameric Molybdenum Sulfide Clusters Activate and Stabilize Dihydrogen as Hydrides

Rachit Khare,[†] Roland Weindl,[†] Andreas Jentys, Karsten Reuter, Hui Shi,* and Johannes A. Lercher*

Cite This: *JACS Au* 2022, 2, 613−622 Read Online

ACCESS | Metrics & More | Article Recommendations | Supporting Information

ABSTRACT: NaY zeolite-encapsulated dimeric (Mo_2S_4) and tetrameric (Mo_4S_4) molybdenum sulfide clusters stabilize hydrogen as hydride binding to Mo atoms. Density functional theory (DFT) calculations and adsorption measurements suggest that stabilization of hydrogen as sulfhydryl (SH) groups, as typical for layered MoS_2, is thermodynamically disfavored. Competitive adsorption of H_2 and ethene on Mo was probed by quantifying adsorbed CO on partly hydrogen and/or ethene covered samples with IR spectroscopy. During hydrogenation, experiment and theory suggest that Mo is covered predominately with ethene and sparsely with hydride. DFT calculations further predict that, under reaction conditions, each Mo_xS_y cluster can activate only one H_2, suggesting that the entire cluster (irrespective of its nuclearity) acts as one active site for hydrogenation. The nearly identical turnover frequencies (24.7 ± 3.3 $mol_{ethane}\cdot h^{-1}\cdot mol_{cluster}^{-1}$), apparent activation energies (31−32 $kJ\cdot mol^{-1}$), and reaction orders (∼0.5 in ethene and ∼1.0 in H_2) show that the active sites in both clusters are catalytically indistinguishable.

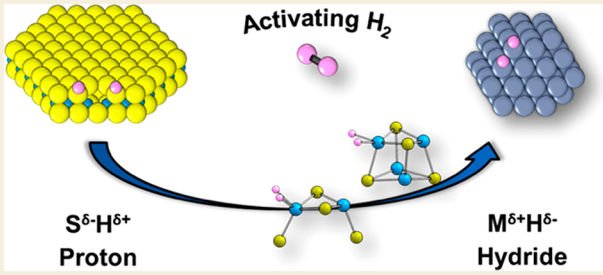

KEYWORDS: *Molybdenum sulfide clusters, hydrogen activation, hydride, IR spectroscopy, density functional theory*

INTRODUCTION

Two-dimensional, nanostructured transition metal sulfides (TMS) have a wide variety of applications in energy conversion.[1] Owing to their robust performance in the presence of heteroatoms, layered TMS materials, primarily based on $Mo(W)S_2$ promoted by Co/Ni, have long been used as hydrodefunctionalization catalysts in hydroprocessing.[2−7] In addition, TMS catalysts show promise for a multitude of processes related to the production of fuels and chemicals,[1] including the upgrading of bioderived feedstocks (e.g., hydrodeoxygenation),[8−10] (reverse) water gas shift (WGS/rWGS),[11,12] and other synthetic approaches including syntheses from CO/CO_2.[13−16] More recently, TMS have been studied as electrocatalysts.[17−21]

Most reactions studied on these catalysts involve H_2 as a reactant on sites that have been characterized by microscopy,[22,23] spectroscopy,[24,25] and adsorption of molecular probes,[26,27] guided and aided by theory.[28−30] The efforts have led to significantly improved catalytic properties, as well as to better atomistic understanding of local structures, and detailed mechanisms for hydrogenation/hydrogenolysis reactions. While the link between these catalysts and enzymes with sulfide based active sites seems intuitive, clear analogies have not been substantiated.[2,6,31]

The impressive progress in the understanding of naturally occurring enzymes featuring metal−sulfur moieties in their active sites allows us now to draw stronger analogies to inorganic materials containing atomistically defined sulfide clusters. The active sites in enzymes are the key to redox and hydrogenation catalysis, such as H^+/H_2 conversion by hydrogenases and nitrogen fixation by nitrogenases.[32−34] To translate this chemistry to nonenzyme systems, several supported (multinuclear) metal−sulfur clusters have been reported, some of which are known to mimic key structural motifs of sulfur-based enzyme cofactors.[35] To make them better accessible for catalytic hydrogenation, inorganic scaffolds are used for stabilization.[14,36]

Activation of H_2 on sulfide materials occurs by dissociative adsorption, resulting in distinct final states for adsorbed hydrogen, e.g., SH groups on sulfide slabs or hydride species on metal sites.[31,37−40] Interestingly, the nitrogenase enzyme's FeMo-cofactor was recently shown to stabilize hydrogen in the form of hydride species; in this case a fraction of adsorbed hydrogen is present as μ-bridging $H^{\delta-}$ on the Fe centers.[34,41−43]

We recently reported Mo_xS_y clusters encapsulated in faujasite-type NaY zeolite with precisely defined nuclearity, geometry, and atomic connectivity.[44−46] Using thermal treatment in sulfiding/reducing atmosphere, two different molecular cluster sizes were stabilized, viz., dimeric Mo_2S_4 and

Received: November 10, 2021
Published: February 9, 2022

https://doi.org/10.1021/jacsau.1c00507
JACS Au 2022, 2, 613−622

tetrameric Mo_4S_4. The latter cluster structurally and electronically resembles the cubane motifs in the nitrogenase enzyme, i.e., the FeMo-cofactor.[32,33] These catalysts exhibited remarkable stability for ethene hydrogenation in the absence of continuous sulfur supply to the reaction feed, while the classic layered MoS_2 catalyst deactivated significantly under the same conditions.[46] This deactivation behavior of conventional MoS_2 catalysts in the absence of sulfur in the feed has been reported extensively in literature.[47−49]

These promising results motivated us to address how these Mo_xS_y clusters activate hydrogen and how their structures dynamically adapt to the reaction environment. Combining IR spectroscopy of adsorbed probe molecules with kinetic measurements and DFT calculations, employing ethene hydrogenation as a model reaction, we develop here the most plausible configurations of Mo_xS_y clusters and the changes in their geometric and electronic properties upon interactions with reactive gases (ethene, H_2, and their mixtures) at low temperature (i.e., 173 K; relevant for CO adsorption measurements) and high temperature (i.e., 473 K; typical hydrogenation reaction temperature). The analyses provide insights into the similarities and differences in H_2 activation and the identity of surface hydrogen species among Mo_xS_y clusters, layered MoS_2, and enzymes containing TMS-based structural motifs, and explains why it is justified to treat the entire cluster, rather than individual Mo atoms, as an active site for hydrogenation catalysis.

■ RESULTS AND DISCUSSION

Active Sites for CO Adsorption and Hydrogenation

Direct spectroscopic evidence for the presence of hydrides on Mo atoms of Mo_xS_y phases has not been achieved so far and appears at present elusive. Thus, we turn to an indirect method to characterize the location and concentration of adsorbed hydrogen, using CO as a probe molecule. CO has been successfully used as a probe for Lewis acid sites (LAS) on TMS.[26,50−52] In this case, CO appears to be an ideal probe. First, as long as CO molecules are not aligned, the wavenumbers of IR bands of CO adsorbed on LAS can be directly related to the electronic properties of the metal sites. Therefore, the observed shift in the band of adsorbed CO allows us to characterize the electronic state of Mo sites in the Mo_xS_y clusters compared to bulk MoS_2. Second, a decrease in the intensity of bands after pre-exposing the catalyst to H_2 and/or ethene indicates blockage of Mo sites by adsorbed hydrogen/ethene. Third, the relative change in the intensity of IR bands (after pre-equilibrating with H_2/ethene) allows to quantitatively estimate the fraction of Mo covered with hydrogen/ethene.

Figure 1 shows the IR spectra of CO adsorbed on Mo_2S_4/NaY, Mo_4S_4/NaY, and MoS_2/γ-Al_2O_3. In addition to the bands attributed to CO adsorbed on the acid sites of the support (i.e., ∼2175 and ∼2125 cm^{-1} for NaY, ∼2195 and ∼2150 cm^{-1} for γ-Al_2O_3), all catalysts showed characteristic broad bands assigned to CO adsorbed on the Mo sites of Mo_xS_y at ∼2035, ∼2075, and 2085 cm^{-1} for the Mo_xS_y/NaY, and at ∼2055, ∼2095, and ∼2105 cm^{-1} for MoS_2/γ-Al_2O_3.[50,53]

In comparison to MoS_2/γ-Al_2O_3, the bands of CO adsorbed on Mo in Mo_xS_y/NaY were red-shifted by ∼20 cm^{-1}, indicating an enhanced electron back-donation from Mo to CO in the case of cluster catalysts. This red-shift suggests a higher electron density in the Mo *d*-orbitals of Mo_xS_y clusters

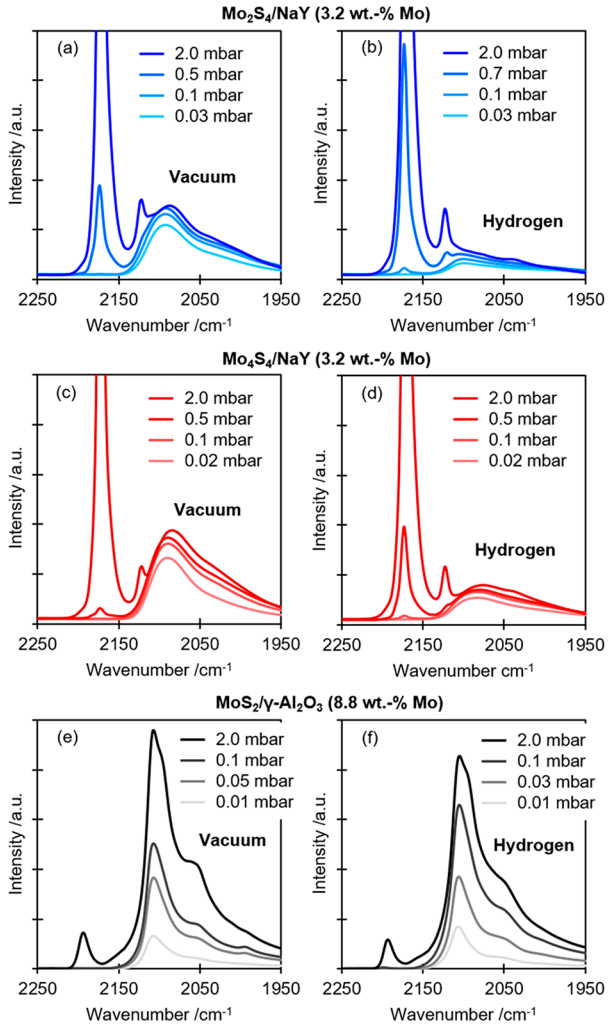

Figure 1. IR spectra of adsorbed CO on Mo_2S_4/NaY (top), Mo_4S_4/NaY (middle), and MoS_2/γ-Al_2O_3 (bottom) after quenching to 173 K in vacuum (left) or H_2 (right). All spectra are normalized to catalyst wafer thickness and mass.

in comparison to the Mo atoms in MoS_2 slabs. It is interesting to note that the observed shift in the wavenumber was identical, suggesting the local electronic environment of Mo to be similar in both dimeric and tetrameric clusters. We also noticed that the amount of adsorbed CO, normalized to Mo content, on the two Mo_xS_y/NaY catalysts (after quenching in vacuum) was comparable: 1455−1708 au on Mo_2S_4/NaY and 1730−1760 au on Mo_4S_4/NaY (Tables S2.1 and S2.2), suggesting that both dimeric and tetrameric clusters can accommodate similar number of CO molecules per Mo and that all Mo sites are accessible to CO adsorption.

We simulated the adsorption of CO on Mo_2S_4 and Mo_4S_4 clusters using DFT. Adsorption of three CO molecules per Mo atom resulted in an octahedral-like coordination environment around the Mo centers (Figure S3.1). This configuration was found to be thermodynamically stable on both clusters (Figure S3.2), thereby confirming the experimental observation that each Mo atom, irrespective of the nuclearity of the cluster it belongs to, can accommodate the same number of CO molecules.

CO binding to the Mo LAS on these NaY-encapsulated Mo_xS_y clusters shows pronounced similarities to CO binding to the nitrogenase enzyme's FeMo-cofactor.[54,55] In both cases,

https://doi.org/10.1021/jacsau.1c00507
JACS Au 2022, 2, 613−622

CO is adsorbed on a metal atom (Mo in our case; Fe in FeMo-cofactor) that itself is coordinated to three nonmetallic atoms (S only in our case; S and C in the FeMo-cofactor) in its first coordination shell. The similarity between these systems is especially intriguing, considering that the activity of nitrogenase enzyme for catalytic hydrogenation of acetylene was shown to be almost completely lost in the presence of CO.[54] Thus, we hypothesize that the Mo centers are at least part of the active site for ethene hydrogenation on these cluster catalysts.

For ethene hydrogenation, representative Mo_2S_4/NaY and Mo_4S_4/NaY catalysts (with ~3.2 wt % Mo) showed similar apparent activation energies (31 ± 1 kJ·mol^{-1} on Mo_2S_4/NaY and 32 ± 3 kJ·mol^{-1} on Mo_4S_4/NaY), similar reaction orders of ~1.0 in H_2 and ~0.5 in C_2H_4 (Figure 2), and virtually identical turnover frequencies (discussed later) indicating that the active sites in both catalysts are catalytically indistinguishable despite different geometries and compositions of the two clusters. It is worth mentioning that X-ray absorption spectroscopy (XAS) measurements verify that the nuclearity of both clusters remains intact under reaction conditions (section S11 in the Supporting Information).

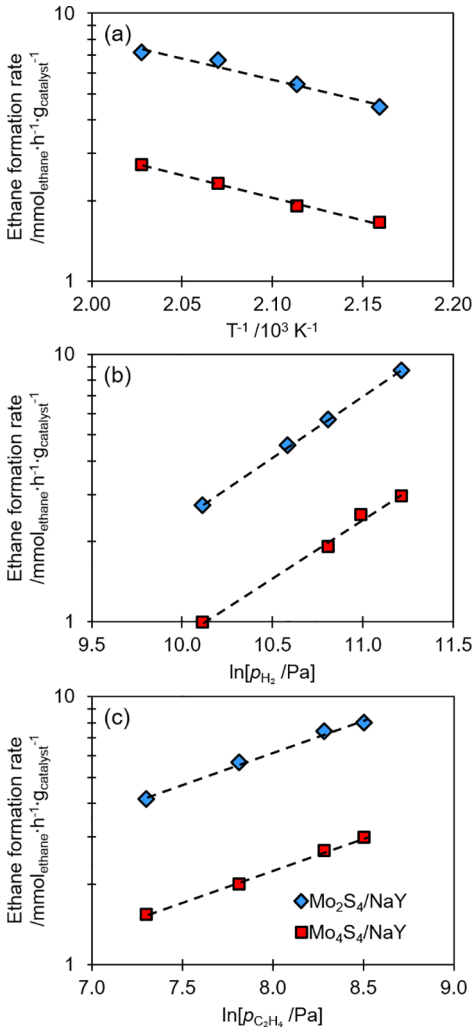

Figure 2. (a) Arrhenius-type plots (T = 463−493 K, p_{H_2} ≈ 49 kPa, $p_{C_2H_4}$ ≈ 2.5 kPa) and (b,c) steady-state ethane formation rates as a function of H_2 pressure (T ≈ 473 K, p_{H_2} = 25−74 kPa, $p_{C_2H_4}$ ≈ 2.5 kPa) and C_2H_4 pressure (T ≈ 473 K, p_{H_2} ≈ 49 kPa, and $p_{C_2H_4}$ = 1.5−5 kPa) on representative Mo_2S_4/NaY and Mo_4S_4/NaY catalysts with ~3.2 wt % Mo.

Hydrogen Adsorption

The amount of CO adsorbed on Mo_xS_y clusters, measured as the relative peak area of corresponding IR bands, decreased when either catalyst was exposed to H_2 (Figure 3). This suggests that hydrogen is adsorbed on the same site as CO, i.e., the Mo atoms. In contrast, the intensity of the bands associated with CO adsorbed on MoS_2/γ-Al_2O_3 were unaffected by exposure to H_2 (decrease by only ~5%). This confirms that hydrogen does not bind to Mo but to sulfur atoms at the perimeter, forming SH groups, on the bulk MoS_2 catalysts.[31,37,38,52]

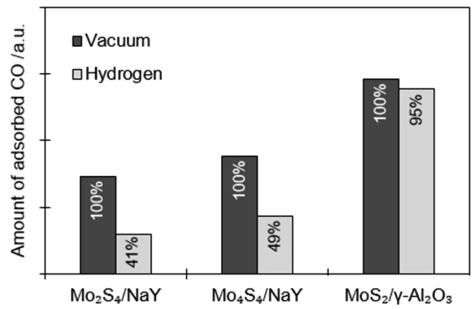

Figure 3. Relative amount of adsorbed CO (normalized to catalyst wafer thickness and mass), measured with IR spectroscopy, on Mo_2S_4/NaY, Mo_4S_4/NaY, and MoS_2/γ-Al_2O_3 after quenching in either vacuum or H_2.

Using 4,6-dimethylpyridine (DMP) to probe weakly Brønsted acidic SH groups via IR bands at ~1650 and ~1625 cm^{-1} (attributed to protonated DMP),[56,57] we had shown that, for Al_2O_3-supported MoS_2, the concentration of SH groups increased after exposure to H_2.[58] However, for Mo_2S_4/NaY (Figure 4), we observed only bands of very low intensity and these bands did not increase after exposure to H_2. Therefore, we conclude that these small bands result from residual Brønsted acid sites (BAS) of the zeolite support and that the Mo_xS_y nanoclusters do not form Brønsted acidic SH groups. In consequence, we conclude that hydrogen is indeed adsorbed on the Mo atoms of Mo_xS_y clusters.

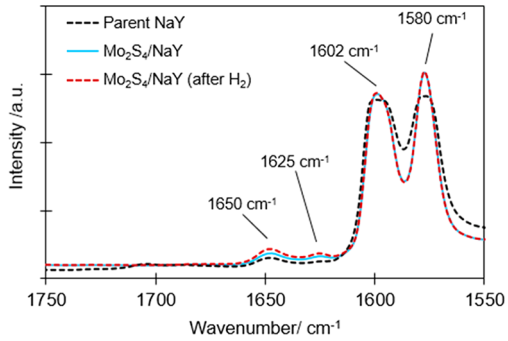

Figure 4. IR spectra of adsorbed 4,6-dimethylpyridine (DMP) on Mo_2S_4/NaY (before and after admission of 1 bar H_2) and parent NaY zeolite. The bands at ~1650 and ~1625 cm^{-1} are assigned to ring vibrations of protonated DMP, the band at ~1602 cm^{-1} to weakly physisorbed DMP, and the band at ~1580 cm^{-1} to DMP physisorbed/adsorbed on zeolite Lewis acid sites.[56−58]

https://doi.org/10.1021/jacsau.1c00507
JACS Au 2022, 2, 613−622

To investigate the adsorption structure further, we optimized (with DFT) the geometries of Mo_2S_4 and Mo_4S_4 clusters with hydrogen dissociatively adsorbed at five distinct locations: a single Mo atom, two different Mo atoms, one Mo and one bridging S atom, two bridging S atoms, and a single bridging S atom. The thermodynamically most stable configuration for both clusters was found to be the one with H_2 dissociatively adsorbed on two different Mo atoms (Figure 5e,f). This configuration was thermodynamically more stable

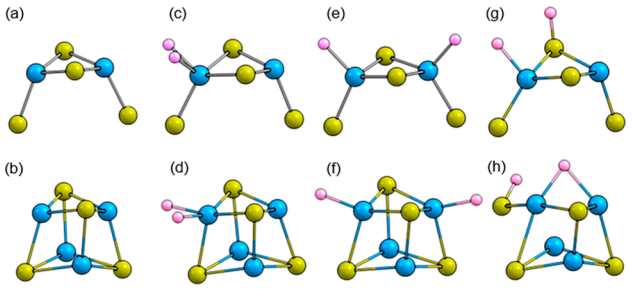

Figure 5. DFT/B3LYP/def2-TZVP-optimized geometries of bare Mo_2S_4 and Mo_4S_4 clusters (a,b) and configurations involving dissociatively adsorbed H_2 on the same Mo atom (c,d), separate Mo atoms (e,f) or one Mo atom and one bridging S atom (g,h). Optimized geometries obtained using PBE0/def2-TZVP were similar. S: yellow; Mo: blue; H: pink.

(Tables S4.1 and S5.1) than the configuration with hydrides stabilized on the same Mo atom (Figure 5c,d). However, the transition from the configuration with hydrides stabilized on a single Mo atom to separate Mo atoms involved a high free energy barrier on both dimeric and tetrameric Mo_xS_y clusters (Figures S4.2 and S5.2).

These high free energy barriers suggest that even though the thermodynamically most stable configuration is the one with hydrides stabilized on separate Mo atoms, these states are kinetically not accessible at reaction conditions. Therefore, under typical reaction conditions, H_2 is likely dissociatively adsorbed on the same Mo atom for both Mo_2S_4 and Mo_4S_4. This adsorbed hydrogen resembles the homolytic H_2 splitting on (noble) metal catalysts[39,40] and points to the similarity to the FeMo cofactor, which similarly is able to stabilize hydrogen as hydride species.[34,42,43,59] We speculate that electronic and structural similarities cause this analogous mode of interaction.

Interestingly, in contrast to the remarkable stability of structures that involved the formation of hydride species, configurations with hydrogen stabilized as SH groups (e.g., Figure 5g,h) were much less stable (Tables S4.1 and S5.1). For the tetrameric cluster, it was not even possible to stabilize hydrogen as SH groups without destroying the structural integrity of the cluster.

The difference between hydrogen activation on Mo_xS_y clusters and bulk MoS_2 however cannot be directly linked to the dimension or the nuclearity of the transition metal sulfide phase as hydrogen was proven to be stabilized as SH groups on metal−organic S-bridged Mo dimers.[60] Therefore, the key difference has to lie within the electronic properties, and more specifically the electron density (or reducibility) of the involved Mo centers. Stabilization of hydrogen in the form of protons is formally an oxidation process and, therefore, requires reduction of the Mo centers.[61] DFT calculations suggested that stabilization of hydrogen as SH groups resulted in electron density transfer from the H to the Mo_xS_y cluster. In contrast, stabilization of hydrogen as hydride species on Mo resulted in electron density transfer from the cluster to the H adatoms (Tables S4.3 and S5.3).

Our DFT models predict that a higher electron density on Mo should favor hydride formation, while a lower electron density on Mo atoms should favor sulfhydryl formation. In the case of extended MoS_2 slabs, upon formation of SH groups, the resulting electron density transfer from hydrogen is likely compensated by multiple Mo atoms and, thus, SH groups as a final state are thermodynamically feasible. DFT calculations additionally predict a barrierless transfer of adsorbed hydrogen from Mo centers to the neighboring S atoms.[31,37,38,62] In the case of zeolite-encapsulated Mo_xS_y nanoclusters, on the other hand, we hypothesize that the more covalent character of Mo−S bonds prevents reduction of these Mo centers perhaps due to a higher local electron density on the Mo atoms.[46,63] For this reason, stabilization of hydrogen as hydride species on these molecular clusters is thermodynamically favored over sulfhydryl group formation. It must be noted in passing that these findings are related to the difference between molybdenum and ruthenium sulfide phases for hydrogen binding observed using inelastic neutron scattering. Sulfhydryl groups were the single hydrogen species on MoS_2 slabs, while a mixture of SH groups and hydride species on the metal atoms of a more metallic RuS_2 phase were observed.[64]

Adsorption of Multiple H_2

As both dimeric and tetrameric Mo_xS_y clusters comprise of multiple Mo atoms, which could potentially adsorb more than one H_2, we simulated the adsorption of multiple H_2 on both dimeric and tetrameric clusters (section S6 in the Supporting Information).

For Mo_2S_4, stable geometries for cases with two dissociatively adsorbed H_2 molecules could not be achieved. The second H_2 could only be stabilized as physisorbed species. For Mo_4S_4, on the other hand, stable geometries could be achieved for clusters accommodating more than one H_2 molecule (Figure S6.1). At 473 K, adsorption of more than one H_2, however, was thermodynamically unfavorable (Figure 6 and Table S6.1). We conclude, therefore, that, at typical reaction temperature, both clusters can only stabilize a single dissociatively adsorbed H_2, thereby acting as one hydro-

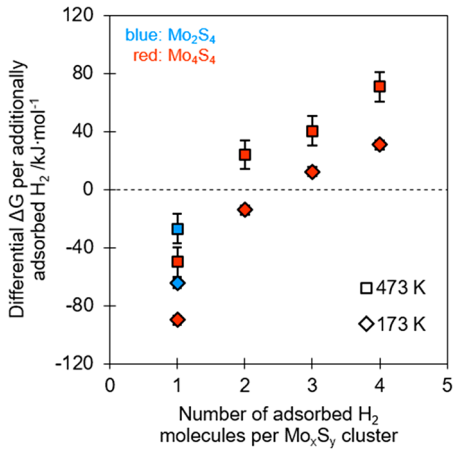

Figure 6. Differential free energy change per additionally adsorbed H_2 on Mo_2S_4 and Mo_4S_4 clusters, computed at T = 473 K and T = 173 K. Error bars correspond to ±1/2D gas-phase translational entropy of H_2.

https://doi.org/10.1021/jacsau.1c00507
JACS Au 2022, 2, 613−622

genation site. Consequentially, the number of Mo_xS_y clusters must be the basis for calculating the turnover frequency for ethene hydrogenation. Applying this for a series of Mo_XS_y/NaY catalysts with varying Mo loading, we observed, as predicted, a constant turnover frequency of 24.7 ± 3.3 $mol_{ethane}\cdot h^{-1}\cdot mol_{cluster}^{-1}$ (Figure 7). It must be noted that a Mo loading of ∼9.7 wt % corresponds to ∼1.6 Mo atoms or ∼0.8 Mo_2S_4 clusters per NaY zeolite supercage.

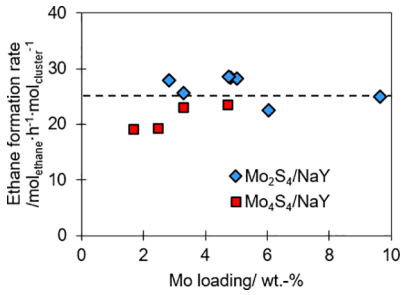

Figure 7. Steady-state ethane formation rates, normalized per cluster, on Mo_2S_4/NaY and Mo_4S_4/NaY catalysts with increasing Mo loading. Reaction conditions: $T \approx 473$ K, $p_{H2} \approx 96$ kPa, and $p_{C2H4} \approx 5$ kPa.

Interestingly, the spin-multiplicity of the (thermodynamically most stable) Mo_4S_4 structure decreased from $\omega = 5$ (i.e., four unpaired electrons) for the bare Mo_4S_4 cluster to $\omega = 3$ (i.e., two unpaired electrons) for the Mo_4S_4 cluster with one adsorbed H_2 and finally to $\omega = 1$ (i.e., no unpaired electrons) for the Mo_4S_4 cluster with two adsorbed H_2 (Tables S6.1 and S6.2). Similarly, the spin-multiplicity of the dimeric cluster also decreased from $\omega = 3$ (i.e., two unpaired electrons) for the bare Mo_2S_4 cluster to $\omega = 1$ (i.e., no unpaired electrons) for the Mo_2S_4 cluster with one adsorbed H_2 molecule (Table S4.1). Based on these observations, we hypothesize that the unpaired electrons on Mo atoms likely interact with hydrogen species upon adsorption.

Ethene Adsorption

Figure 8 shows the IR spectra of adsorbed CO on Mo_xS_y/NaY catalysts after quenching to 173 K in ethene atmosphere. Quantitative analysis of the IR spectra shows that the concentration of CO adsorbed on Mo Lewis acid sites was reduced to ∼14% on Mo_2S_4/NaY and to ∼11% on Mo_4S_4/NaY after equilibration with ethene at 173 K (Figure 9 and Table S2.2). This suggests that in the presence of ethene a significantly higher fraction of Mo (as compared to the experiments with H_2 pretreatment) becomes inaccessible to CO, thereby suggesting that the coverage of ethene must be higher than that of hydrogen on Mo under the tested conditions.

DFT calculations of the adsorption of ethene on Mo_2S_4 and Mo_4S_4 (section S7 and S8 in the Supporting Information) showed that ethene could not be stabilized on the S atoms of Mo_xS_y clusters but only on Mo atoms. However, in contrast to hydrogen adsorption, adsorption of multiple ethene molecules was thermodynamically favored on both Mo_2S_4 and Mo_4S_4 (Figure 10).

Based on free energy calculations at 173 and 473 K, the configurations with two chemisorbed ethene molecules on Mo_2S_4 (Figure 11a) and four chemisorbed ethene molecules on Mo_4S_4 (Figure 11c) were thermodynamically most favored. The differential standard free energy change, however, decreased with the adsorption of each additional ethene molecule. DFT therefore predicts that, for CO adsorption experiments, a significant fraction of Mo atoms is expected to be covered by ethene. This prediction agrees with IR spectroscopy measurements that showed that ∼86% and ∼89% of Mo atoms were inaccessible to CO once the cluster had been in contact with ethene (Figure 9 and Table S2.2).

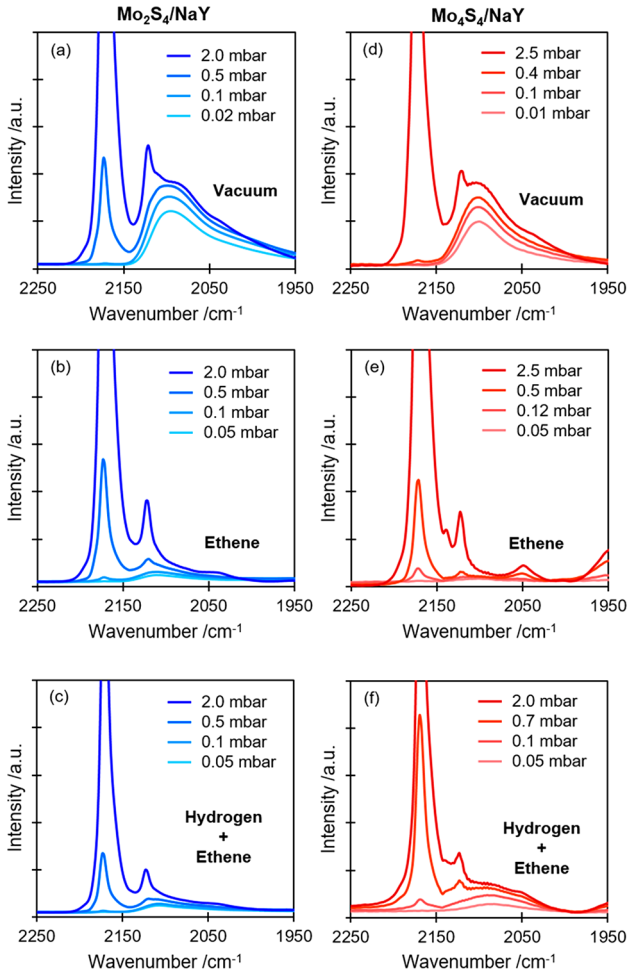

Figure 8. IR spectra of adsorbed CO on Mo_2S_4/NaY (left) and Mo_4S_4/NaY (right) after quenching to 173 K in vacuum (top), ethene (middle), or a mixture of hydrogen and ethene (bottom). All spectra are normalized to catalyst wafer thickness and mass.

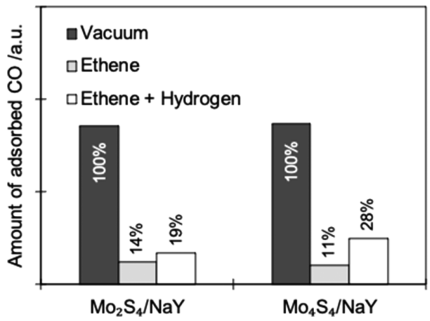

Figure 9. Relative amount of adsorbed CO (normalized to catalyst wafer thickness and mass), measured with IR spectroscopy, on Mo_2S_4/NaY and Mo_4S_4/NaY after quenching in vacuum, ethene, or a mixture of ethene and hydrogen.

https://doi.org/10.1021/jacsau.1c00507
JACS Au 2022, 2, 613−622

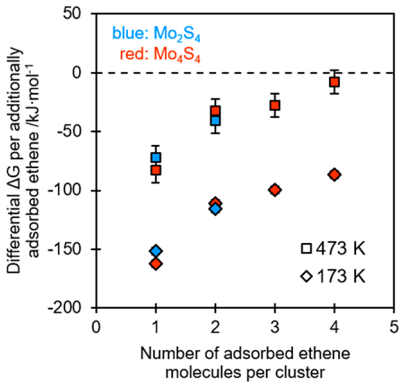

Figure 10. Differential free energy change per additionally adsorbed ethene molecule on Mo_2S_4 and Mo_4S_4 clusters, computed at T = 473 K and T = 173 K. Error bars correspond to ±1/2D gas-phase translational entropy of ethene.

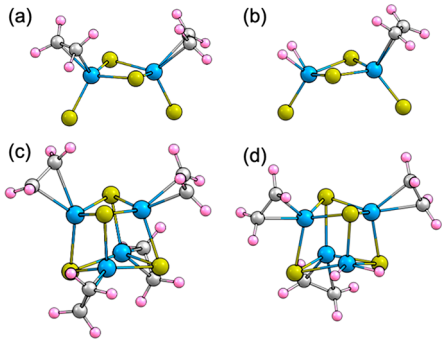

Figure 11. DFT/B3LYP/def2-TZVP-optimized geometries of a Mo_2S_4 cluster with (a) two adsorbed ethene molecules and (b) one ethene and one hydrogen molecule, and a Mo_4S_4 cluster with (c) four adsorbed ethene molecules and (d) one hydrogen and three ethene molecules. S: yellow; Mo: blue; C: gray; H: pink.

Competitive Adsorption between Ethene and Hydrogen

Using IR spectroscopy and DFT calculations, we showed above that both H_2 and ethene are adsorbed on the Mo atoms of the Mo_xS_y clusters. As both ethene and H_2 are simultaneously present during ethene hydrogenation and compete for the same sites, we turned to the IR spectra of adsorbed CO after quenching the samples to 173 K in a typical reaction mixture containing ∼960 mbar bar H_2 and ∼50 mbar ethene, resulting in blocking of ∼81% Mo sites for Mo_2S_4/NaY and ∼72% Mo sites for Mo_4S_4/NaY (Figure 9 and Table S2.2).

DFT (sections S9 and S10 in the Supporting Information) showed that the Mo_2S_4 cluster with one ethene molecule and one H_2 molecule adsorbed on different Mo atoms (Figure 11b) was thermodynamically less stable than the thermodynamically most stable configuration with two adsorbed ethene molecules (Figure 11a).

Similarly, for the tetrameric cluster, the configuration with one hydrogen and three ethene molecules adsorbed on separate Mo atoms (Figure 11d) was higher in free energy in comparison to the thermodynamically most stable configuration with four adsorbed ethene molecules (Figure 11c). As this holds true at 173 K as well as at 473 K, we conclude that the clusters with at least one dissociatively adsorbed H_2 (i.e., the ones likely functioning as starting point for hydrogenation) are a minority species under reaction conditions. Note that this agrees well with the fact that ethene hydrogenation had a first order pressure dependence in H_2 on both Mo_2S_4/NaY and Mo_4S_4/NaY catalysts (Figure 2b).

Given the large distance between Mo atoms on Mo_xS_y clusters, and consequentially between the reactants adsorbed on these sites (Figure 11b,d), we hypothesize that the reaction between adsorbed ethene and adsorbed H_2 species to form ethane, i.e., Langmuir−Hinshelwood (LH) type mechanism, is unlikely. We instead propose that the reaction proceeds via an Eley−Rideal (ER) type mechanism, wherein ethene weakly adsorbed in the zeolite pores reacts with an adsorbed hydrogen. The fractional reaction order in ethene (instead of unity as expected for ER type reactions) is attributed to the negative influence of the ethene partial pressure on the hydrogen coverage with both ethene and hydrogen competing for the same sites.

DFT simulations for LH-type (involving an adsorbed H_2 and an adsorbed ethene) and ER-type (involving as adsorbed H_2 and a gas-phase ethene) reaction pathways on the Mo_2S_4 cluster are presented in section S12 in the Supporting Information. The standard enthalpic barriers for the LH-type reaction pathway were computed to be higher than that for the ER-type reaction pathway (Figures S12.1 and S12.2). The DFT calculations, therefore, support our hypothesis that the ER-type reaction mechanism (as opposed to LH-type reaction mechanism) likely proceeds on these zeolite pore stabilized molybdenum sulfide clusters.

■ CONCLUSIONS

NaY zeolite-encapsulated Mo_xS_y clusters adsorb H_2 dissociatively, binding both H atoms to a single Mo atom. DFT calculations suggest that this adsorption structure is caused by a high barrier to distribute the H atoms evenly among all Mo atoms of the cluster. Adsorption of hydrogen as hydrides contrasts the stabilization of hydrogen as sulfhydryl groups on the edge of conventional MoS_2 slabs. The difference is attributed to the easier reducibility of Mo in the larger MoS_2 slabs.

Both dimeric and tetrameric Mo_xS_y cluster catalysts show stable rates of hydrogenation scaling with the concentration of clusters in the catalyst, independent of the cluster nuclearity. This is also reflected by DFT calculations indicating that only one hydrogen can be dissociatively adsorbed per cluster under reaction conditions. The nature of the active site is concluded to be identical for both clusters, i.e., a single Mo center, as demonstrated by constant activation energies and reaction orders in H_2 and ethene on both Mo_2S_4/NaY and Mo_4S_4/NaY catalysts.

Thus, experiments and theory suggest jointly that active sites in both dimeric and tetrameric catalysts are catalytically indistinguishable for ethene hydrogenation. Theory and experiment also show that ethene, H_2, and CO, competitively adsorb on Mo similarly to the situation reported for the FeMo sulfide cluster in nitrogenase. As ethene adsorbs more strongly than H_2 on both cluster catalysts, it is predicted to be the most abundant surface species under reaction conditions. Ethene hydrogenation is postulated to proceed via Eley−Rideal type mechanism, with a weakly adsorbed ethene in the zeolite pores reacting with an adsorbed hydrogen. The reaction between adsorbed ethene and adsorbed hydrogen, i.e., the Langmuir−Hinshelwood type pathway, was found to have a high enthalpic barrier owing to large distance between the Mo atoms in these clusters.

https://doi.org/10.1021/jacsau.1c00507
JACS Au 2022, 2, 613−622

EXPERIMENTAL AND COMPUTATIONAL METHODS

Catalyst Precursor Preparation

$MoS_2/\gamma\text{-}Al_2O_3$ catalyst precursors were prepared by incipient wetness impregnation of $\gamma\text{-}Al_2O_3$ (provided by the Chevron company) with an ammonium heptamolybdate (99.98% purity; Sigma-Aldrich) solution of appropriate concentration. The impregnated sample was dried at 383 K overnight followed by calcination in 100 mL·min^{-1} synthetic air (temperature ramp: 5 K·min^{-1} to 673 K, hold for 2 h).

Carbonyl-based catalyst precursors were prepared by chemical vapor deposition (CVD). Approximately 200 mg of NaY (Zeolyst CBV100; Si/Al ∼ 2.5; pelletized and sieved to 250−355 μm) was treated under reduced pressure (10^{-2} mbar) at elevated temperatures (temperature ramp: 5 K·min^{-1} to 408 K, held for 2 h; 5 K·min^{-1} to 503 K, held for 2 h; 5 K·min^{-1} to 653 K, held for 1 h) to carefully remove adsorbed water. Molybdenum hexacarbonyl (>99.9% purity; Sigma-Aldrich) was loaded on the dried zeolite at room temperature under static conditions for a defined amount of time. In the final step, the catalyst precursors were treated under reduced pressure (10^{-2} mbar) for 10 min to remove physisorbed $Mo(CO)_6$. All carbonyl-based precursors were stored in a glovebox to avoid exposure to air/moisture at any time.

Catalyst Preparation

$MoS_2/\gamma\text{-}Al_2O_3$ and NaY-encapsulated cluster catalysts were prepared in a lab-scale plug flow reactor (quartz glass tube; 4 mm i.d.). Bronkhorst mass flow controllers were used to regulate gas flow rates. To avoid formation of hotspots, all precursors were diluted 1/10 in SiC (sieved to 500−1000 μm) and placed in the quartz tube supported with quartz wool on both sides. The precursors prepared via incipient wetness impregnation were sulfided in a stream of 20 mL·min^{-1} H_2S (10% v/v in H_2) at ambient pressure (temperature ramp: 5 K·min^{-1} to 673 K, held for 16 h). Precursors prepared via CVD were also sulfided in a flow of 20 mL·min^{-1} H_2S (10% v/v in H_2) at ambient pressure (temperature ramp: 5 K·min^{-1} to 673 K, held for 2 h) to form sulfided Mo_xS_y/NaY catalyst (previously shown to be primarily composed of dimeric Mo_2S_4 clusters and denoted as Mo_2S_4/NaY).[46] The Mo_2S_4/NaY catalyst was then treated in a stream of pure H_2 (temperature ramp: 5 K·min^{-1} to 673 K, held for 2 h) to obtain the reduced Mo_xS_y/NaY catalyst (previously shown to be primarily comprised of tetrameric Mo_4S_4 clusters and denoted as Mo_4S_4/NaY).[46] After thermal treatments, all catalysts were purged with N_2 for 30 min prior to any catalytic reactions.

Catalytic Reactions

All catalytic reactions were also performed in the lab-scale plug flow reactor. Ethene hydrogenation was studied at ∼473 K and ambient pressure with a H_2/ethene volumetric ratio of ∼20. The product stream composition was analyzed by online gas chromatography using an Agilent 7890B GC. Ethane formation rates were determined using space−time yields under differential conditions after the catalysts reached a stable steady state (after ∼24 h). External mass transport limitations have been excluded for the applied reaction conditions by varying the amount of loaded catalyst and its particle size. Limitations by internal mass transport were excluded owing to the small size of Mo_xS_y clusters (∼5 Å for Mo_4S_4) and reactants/products in comparison to the diameter of the NaY zeolite supercages (∼12 Å) and the pore openings (∼7 Å).

Infrared (IR) Spectroscopy of Adsorbed Probe Molecules

IR spectroscopy of adsorbed probe molecules was performed using a Nicolet 6700 IR spectrometer with a resolution of 4 cm^{-1}. The catalyst materials were ground and pressed into self-supporting wafers (∼5 mg·cm^{-2}). The catalyst wafers were first sulfided/reduced in a stream of 20 mL·min^{-1} H_2S (10% v/v in H_2) or 20 mL·min^{-1} H_2 at ambient pressure (temperature ramp: 5 K·min^{-1} to 673 K, held for 2 h). Then, for activation, a treatment in H_2 (4 cycles, total of 24 h) at 473 K each followed by evacuation at 10^{-6} mbar for 30 min was applied to all samples.

CO adsorption was performed on activated samples after cooling to 173 K using liquid nitrogen. The samples were examined after cooling in either H_2, ethene, a mixture of H_2 and ethene, or high vacuum. In a first run, after cooling to 173 K (by skipping the last evacuation cycle) in either H_2, ethene, or a mixture of H_2 and ethene, CO adsorption isotherms were obtained by applying controlled doses of CO ranging from 0.01 to 2 mbar. After this, CO and other adsorbed gases were desorbed at room temperature under high vacuum (10^{-7} mbar). Subsequently, the samples were thermally treated at 473 K for 1 h and cooled down to 173 K again under high vacuum (10^{-7} mbar) before the second run of CO adsorption. Possible errors caused by different thicknesses of the catalyst wafers are prevented in this procedure as multiple series of measurements are conducted on the same wafer. In lieu of molar extinction coefficients for bands of CO adsorbed on cluster catalysts, we analyzed the areas normalized to wafer thickness for all experiments.

IR spectroscopy of adsorbed 4,6-dimethylpyridine (DMP) was performed on the activated samples at 323 K by applying small doses of DMP (up to 0.5 mbar) into the IR cell and equilibrating for 0.5 h. A second spectrum was taken after exposing the catalyst to an additional ∼1 bar of H_2 and equilibrating for another 0.5 h.

All IR spectra were background corrected using the OMNIC software package, and they are presented as difference spectra against the reference spectra at 10^{-7} mbar.

Computational Details

Unrestricted Kohn−Sham (UKS) DFT calculations were performed on gas-phase Mo_xS_y clusters using the Orca quantum chemistry package version 4.2.[65−67] The calculations were performed using two hybrid exchange-correlational functionals: B3LYP and PBE0. Relativistic effects were taken into account by zeroth-order regular relativistic approximations (ZORA), and Grimme's atom-pairwise dispersion correction with the Becke−Johnson damping scheme (D3BJ) was used for dispersion corrections.[68−70] Relativistically recontracted versions of the all-electron Ahlrichs def2 basis sets with triple-ζ polarization functions, ZORA-def2-TZVP, were employed for geometry optimization and vibrational frequency calculations, while ZORA-def2-TZVPP basis-sets were employed for single-point energy (SPE) calculations.[71] The hybrid functionals were employed with RIJCOSX approximation to speed up the calculations, and general auxiliary basis sets SARC/J were used for this purpose.[72−77] The RIJCOSX approach incorporates the resolution-of-identity (RI) approximation for the evaluation of the Coulomb matrices and the chain-of-spheres algorithm for the formation of the exchange-type matrices.[78−80] The core electrons ($1s^22s^22p^63s^23p^63d^{10}$ for Mo, $1s^22s^22p^6$ for S, $1s^2$ for C, and none for H) were kept frozen during geometry optimization and vibrational frequency calculations. The Hirshfeld charge populations and Mayer bond orders were computed for the optimized geometries. Standard thermodynamics equations were used for computing the free energy and free enthalpy of different structures, and the methodology is presented in detail in section S1 in the Supporting Information.

ASSOCIATED CONTENT

Supporting Information

The Supporting Information is available free of charge at https://pubs.acs.org/doi/10.1021/jacsau.1c00507.

Additional experimental and computation details, detailed results from DFT calculations, X-ray absorption spectroscopy results, infrared spectroscopy results (PDF)

AUTHOR INFORMATION

Corresponding Authors

Hui Shi − *School of Chemistry and Chemical Engineering, Yangzhou University, Yangzhou 225009 Jiangsu, China;*

https://doi.org/10.1021/jacsau.1c00507
JACS Au 2022, 2, 613−622

orcid.org/0000-0003-1180-7443; Email: shihui@yzu.edu.cn

Johannes A. Lercher − *Department of Chemistry and Catalysis Research Center, Technical University of Munich, 85747 Garching, Germany; Institute for Integrated Catalysis, Pacific Northwest National Laboratory, Richland, Washington 99354, United States;* orcid.org/0000-0002-2495-1404; Email: johannes.lercher@pnnl.gov, johannes.lercher@ch.tum.de

Authors

Rachit Khare − *Department of Chemistry and Catalysis Research Center, Technical University of Munich, 85747 Garching, Germany;* orcid.org/0000-0002-1519-5184

Roland Weindl − *Department of Chemistry and Catalysis Research Center, Technical University of Munich, 85747 Garching, Germany;* orcid.org/0000-0002-6174-0171

Andreas Jentys − *Department of Chemistry and Catalysis Research Center, Technical University of Munich, 85747 Garching, Germany;* orcid.org/0000-0001-5877-5042

Karsten Reuter − *Department of Chemistry and Catalysis Research Center, Technical University of Munich, 85747 Garching, Germany; Fritz Haber Institute of the Max Planck Society, 14195 Berlin, Germany;* orcid.org/0000-0001-8473-8659

Complete contact information is available at: https://pubs.acs.org/10.1021/jacsau.1c00507

Author Contributions

[†]R.K. and R.W. contributed equally. The manuscript was written through contributions of all authors. All authors have given approval to the final version of the manuscript.

Funding

This work was funded in part by the Chevron Energy Technology Company.

Notes

The authors declare no competing financial interest.

■ ACKNOWLEDGMENTS

The authors thank Dr. A. Kuperman and Dr. A. Brait (Chevron) and Prof. Takeshi Kubota (Shimane University, Japan) for fruitful discussions. J.A.L. was supported by the U.S. Department of Energy (DOE), Office of Science, Office of Basic Energy Sciences, Division of Chemical Sciences, Geosciences and Biosciences (Transdisciplinary Approaches to Realize Novel Catalytic Pathways to Energy Carriers, FWP 47319). The authors gratefully acknowledge the Leibniz Supercomputing Center for funding this project by providing computing time on their Linux-Cluster. The XAS measurements were performed at the P65 beamline of DESY (Hamburg, Germany), a member of the Helmholtz Association HGF, as a part of the proposal I-20200919. The authors would like to acknowledge support from Dr. Edmund Welter and other staff from the P65 beamline.

■ REFERENCES

(1) Mao, J.; Wang, Y.; Zheng, Z.; Deng, D. The rise of two-dimensional MoS_2 for catalysis. *Frontiers of Physics* **2018**, *13* (4), 1−19.

(2) Prins, R. Hydrotreating. In *Handbook of Heterogeneous Catalysis*; Ertl, G., Knözinger, H., Schüth, F., Weitkamp, J., Eds.; John Wiley & Sons: 2008; pp 2695−2718.

(3) Weisser, O.; Landa, S. *Sulphide catalysts, their properties and applications*; Pergamon Press: Oxford, 2013.

(4) Topsøe, H.; Clausen, B. S. Importance of Co-Mo-S type structures in hydrodesulfurization. *Catalysis Reviews* **1984**, *26* (3−4), 395−420.

(5) Chianelli, R. R.; Berhault, G.; Torres, B. Unsupported transition metal sulfide catalysts: 100 years of science and application. *Catal. Today* **2009**, *147* (3), 275−286.

(6) Eijsbouts, S.; Mayo, S. W.; Fujita, K. Unsupported transition metal sulfide catalysts: From fundamentals to industrial application. *Applied Catalysis A: General* **2007**, *322*, 58−66.

(7) Prins, R.; Egorova, M.; Röthlisberger, A.; Zhao, Y.; Sivasankar, N.; Kukula, P. Mechanisms of hydrodesulfurization and hydrodenitrogenation. *Catal. Today* **2006**, *111* (1), 84−93.

(8) Mortensen, P. M.; Grunwaldt, J.-D.; Jensen, P. A.; Knudsen, K. G.; Jensen, A. D. A review of catalytic upgrading of bio-oil to engine fuels. *Applied Catalysis A: General* **2011**, *407* (1−2), 1−19.

(9) Wang, H.; Male, J.; Wang, Y. Recent advances in hydrotreating of pyrolysis bio-oil and its oxygen-containing model compounds. *ACS Catal.* **2013**, *3* (5), 1047−1070.

(10) Bui, V. N.; Laurenti, D.; Afanasiev, P.; Geantet, C. Hydrodeoxygenation of guaiacol with CoMo catalysts. Part I: Promoting effect of cobalt on HDO selectivity and activity. *Applied Catalysis B: Environmental* **2011**, *101* (3−4), 239−245.

(11) Hou, P.; Meeker, D.; Wise, H. Kinetic studies with a sulfur-tolerant water gas shift catalyst. *J. Catal.* **1983**, *80* (2), 280−285.

(12) Lund, C. R. F. Effect of adding Co to MoS_2/Al_2O_3 upon the kinetics of the water−gas shift. *Ind. Eng. Chem. Res.* **1996**, *35* (9), 3067−3073.

(13) Hu, J.; Yu, L.; Deng, J.; Wang, Y.; Cheng, K.; Ma, C.; Zhang, Q.; Wen, W.; Yu, S.; Pan, Y.; et al. Sulfur vacancy-rich MoS_2 as a catalyst for the hydrogenation of CO_2 to methanol. *Nature Catalysis* **2021**, *4* (3), 242−250.

(14) Taniguchi, M.; Ishii, Y.; Murata, T.; Tatsumi, T.; Hidai, M. Preparation of zeolites incorporating molybdenum sulfide clusters with high C_2 hydrocarbon selectivity in Co-H_2 reactions. *J. Chem. Soc., Chem. Commun.* **1995**, No. 24, 2533−2534.

(15) Zhu, Q.; Wegener, S. L.; Xie, C.; Uche, O.; Neurock, M.; Marks, T. J. Sulfur as a selective 'soft' oxidant for catalytic methane conversion probed by experiment and theory. *Nat. Chem.* **2013**, *5* (2), 104−109.

(16) Santos, V. P.; Van Der Linden, B.; Chojecki, A.; Budroni, G.; Corthals, S.; Shibata, H.; Meima, G. R.; Kapteijn, F.; Makkee, M.; Gascon, J. Mechanistic insight into the synthesis of higher alcohols from syngas: the role of K promotion on MoS_2 catalysts. *ACS Catal.* **2013**, *3* (7), 1634−1637.

(17) Hinnemann, B.; Moses, P. G.; Bonde, J.; Jørgensen, K. P.; Nielsen, J. H.; Horch, S.; Chorkendorff, I.; Nørskov, J. K. Biomimetic hydrogen evolution: MoS_2 nanoparticles as catalyst for hydrogen evolution. *J. Am. Chem. Soc.* **2005**, *127* (15), 5308−5309.

(18) Jaramillo, T. F.; Jørgensen, K. P.; Bonde, J.; Nielsen, J. H.; Horch, S.; Chorkendorff, I. Identification of active edge sites for electrochemical H_2 evolution from MoS_2 nanocatalysts. *Science* **2007**, *317* (5834), 100−102.

(19) Li, P.; Yang, Z.; Shen, J.; Nie, H.; Cai, Q.; Li, L.; Ge, M.; Gu, C.; Chen, X. a.; Yang, K.; et al. Subnanometer molybdenum sulfide on carbon nanotubes as a highly active and stable electrocatalyst for hydrogen evolution reaction. *ACS Appl. Mater. Interfaces* **2016**, *8* (5), 3543−3550.

(20) Tran, P. D.; Tran, T. V.; Orio, M.; Torelli, S.; Truong, Q. D.; Nayuki, K.; Sasaki, Y.; Chiam, S. Y.; Yi, R.; Honma, I.; et al. Coordination polymer structure and revisited hydrogen evolution catalytic mechanism for amorphous molybdenum sulfide. *Nat. Mater.* **2016**, *15* (6), 640−646.

(21) Wang, H.; Tsai, C.; Kong, D.; Chan, K.; Abild-Pedersen, F.; Nørskov, J. K.; Cui, Y. Transition-metal doped edge sites in vertically aligned MoS_2 catalysts for enhanced hydrogen evolution. *Nano Research* **2015**, *8* (2), 566−575.

(22) Helveg, S.; Lauritsen, J. V.; Laegsgaard, E.; Stensgaard, I.; Norskov, J. K.; Clausen, B. S.; Topsoe, H.; Besenbacher, F. Atomic-scale structure of single-layer MoS_2 nanoclusters. *Phys. Rev. Lett.* **2000**, *84* (5), 951−954.
(23) Kisielowski, C.; Ramasse, Q. M.; Hansen, L. P.; Brorson, M.; Carlsson, A.; Molenbroek, A. M.; Topsøe, H.; Helveg, S. Imaging MoS_2 nanocatalysts with single-atom sensitivity. *Angew. Chem., Int. Ed.* **2010**, *49* (15), 2708−2710.
(24) Bouwens, S. M. A. M.; Van Veen, J. A. R.; Koningsberger, D. C.; De Beer, V. H. J.; Prins, R. EXAFS determination of the structure of cobalt in carbon-supported cobalt and cobalt-molybdenum sulfide hydrodesulfurization catalysts. *J. Phys. Chem.* **1991**, *95* (1), 123−134.
(25) Wagenhofer, M. F.; Shi, H.; Gutiérrez, O. Y.; Jentys, A.; Lercher, J. A. Enhancing hydrogenation activity of Ni-Mo sulfide hydrodesulfurization catalysts. *Science Advances* **2020**, *6* (19), eaax5331.
(26) Oliviero, L.; Travert, A.; Garcia, E. D.; Chen, J.; Maugé, F. Catalysis by sulfides: Advanced IR/CO spectroscopy for the identification of the most active sites in hydrodesulfurization reactions. *J. Catal.* **2021**, *403*, 87.
(27) Vogelgsang, F.; Shi, H.; Lercher, J. A. Toward quantification of active sites and site-specific activity for polyaromatics hydrogenation on transition metal sulfides. *J. Catal.* **2021**, *403*, 98.
(28) Casalongue, H. G. S.; Benck, J. D.; Tsai, C.; Karlsson, R. K. B.; Kaya, S.; Ng, M. L.; Pettersson, L. G. M.; Abild-Pedersen, F.; Nørskov, J. K.; Ogasawara, H.; et al. Operando characterization of an amorphous molybdenum sulfide nanoparticle catalyst during the hydrogen evolution reaction. *J. Phys. Chem. C* **2014**, *118* (50), 29252−29259.
(29) Gaur, A.; Hartmann Dabros, T. M.; Høj, M.; Boubnov, A.; Prüssmann, T.; Jelic, J.; Studt, F.; Jensen, A. D.; Grunwaldt, J.-D. Probing the active sites of MoS_2 based hydrotreating catalysts using modulation excitation spectroscopy. *ACS Catal.* **2019**, *9* (3), 2568−2579.
(30) Šarić, M.; Rossmeisl, J.; Moses, P. G. Modeling the adsorption of sulfur containing molecules and their hydrodesulfurization intermediates on the Co-promoted MoS_2 catalyst by DFT. *Journal of catalysis* **2018**, *358*, 131−140.
(31) Byskov, L. S.; Bollinger, M.; Nørskov, J. K.; Clausen, B. S.; Topsøe, H. Molecular aspects of the H_2 activation on MoS_2 based catalysts — the role of dynamic surface arrangements. *J. Mol. Catal. A: Chem.* **2000**, *163* (1), 117−122.
(32) Einsle, O.; Tezcan, F. A.; Andrade, S. L.; Schmid, B.; Yoshida, M.; Howard, J. B.; Rees, D. C. Nitrogenase MoFe-protein at 1.16 Å resolution: a central ligand in the FeMo-cofactor. *Science* **2002**, *297* (5587), 1696−1700.
(33) Howard, J. B.; Rees, D. C. Structural basis of biological nitrogen fixation. *Chem. Rev.* **1996**, *96* (7), 2965−2982.
(34) Hoeke, V.; Tociu, L.; Case, D. A.; Seefeldt, L. C.; Raugei, S.; Hoffman, B. M. High-resolution ENDOR spectroscopy combined with quantum chemical calculations reveals the structure of nitrogenase Janus intermediate E_4(4H). *J. Am. Chem. Soc.* **2019**, *141* (30), 11984−11996.
(35) Weigand, W.; Schollhammer, P. *Bioinspired catalysis: metal-sulfur complexes*; Wiley-VCH: Weinheim, 2014.
(36) Taniguchi, M.; Imamura, D.; Ishige, H.; Ishii, Y.; Murata, T.; Hidai, M.; Tatsumi, T. Hydrodesulfurization of benzothiophene over zeolite-supported catalysts prepared from Mo and Mo-Ni sulfide clusters. *J. Catal.* **1999**, *187* (1), 139−150.
(37) Hensen, E. J. M.; Lardinois, G. M. H. J.; de Beer, V. H. J.; van Veen, J. A. R.; van Santen, R. A. Hydrogen−deuterium equilibration over transition metal sulfide catalysts: On the synergetic effect in CoMo catalysts. *J. Catal.* **1999**, *187* (1), 95−108.
(38) Breysse, M.; Furimsky, E.; Kasztelan, S.; Lacroix, M.; Perot, G. Hydrogen activation by transition metal sulfides. *Catalysis Reviews* **2002**, *44* (4), 651−735.
(39) Makolkin, N. V.; Kim, H. U.; Paukshtis, E. A.; Jae, J.; Bal'zhinimaev, B. S. Reactivity of platinum hydrides in the selective hydrogenation of acetic acid on Pt-ReO_x/TiO_2 catalysts. *Catalysis in Industry* **2020**, *12* (4), 316−322.
(40) Möbus, K.; Grünewald, E.; Wieland, S. D.; Parker, S. F.; Albers, P. W. Palladium-catalyzed selective hydrogenation of nitroarenes: Influence of platinum and iron on activity, particle morphology and formation of β-palladium hydride. *J. Catal.* **2014**, *311*, 153−160.
(41) Doan, P. E.; Telser, J.; Barney, B. M.; Igarashi, R. Y.; Dean, D. R.; Seefeldt, L. C.; Hoffman, B. M. ^{57}Fe ENDOR spectroscopy and 'electron inventory' analysis of the nitrogenase E_4 intermediate suggest the metal-ion core of FeMo-cofactor cycles through only one redox couple. *J. Am. Chem. Soc.* **2011**, *133* (43), 17329−17340.
(42) Igarashi, R. Y.; Laryukhin, M.; Dos Santos, P. C.; Lee, H.-I.; Dean, D. R.; Seefeldt, L. C.; Hoffman, B. M. Trapping H-bound to the nitrogenase FeMo-cofactor active site during H_2 evolution: Characterization by ENDOR spectroscopy. *J. Am. Chem. Soc.* **2005**, *127* (17), 6231−6241.
(43) Van Stappen, C.; Davydov, R.; Yang, Z.-Y.; Fan, R.; Guo, Y.; Bill, E.; Seefeldt, L. C.; Hoffman, B. M.; DeBeer, S. Spectroscopic description of the E_1 State of Mo nitrogenase based on Mo and Fe X-ray absorption and Mössbauer studies. *Inorg. Chem.* **2019**, *58* (18), 12365−12376.
(44) Okamoto, Y. Novel molecular approaches to the structure−activity relationships and unique characterizations of Co-Mo sulfide hydrodesulfurization catalysts for the production of ultraclean fuels. *Bull. Chem. Soc. Jpn.* **2014**, *87* (1), 20−58.
(45) Okamoto, Y.; Katsuyama, H.; Yoshida, K.; Nakai, K.; Matsuo, M.; Sakamoto, Y.; Yu, J.; Terasaki, O. Dispersion and location of molybdenum sulfides supported on zeolite for hydrodesulfurization. *Journal of the Chemical Society, Faraday Transactions* **1996**, *92* (22), 4647−4656.
(46) Weindl, R.; Khare, R.; Kovarik, L.; Jentys, A.; Reuter, K.; Shi, H.; Lercher, J. A. Zeolite-stabilized di- and tetranuclear molybdenum sulfide clusters form stable catalytic hydrogenation sites. *Angew. Chem., Int. Ed.* **2021**, *60* (17), 9301−9305.
(47) Topsøe, H.; Clausen, B. S.; Massoth, F. E. Hydrotreating catalysis. In *Catalysis*; Springer: Berlin, 1996; pp 1−269.
(48) Guichard, B.; Roy-Auberger, M.; Devers, E.; Pichon, C.; Legens, C. Characterization of aged hydrotreating catalysts. Part II: The evolution of the mixed phase. Effects of deactivation, activation and/or regeneration. *Applied Catalysis A: General* **2009**, *367* (1−2), 9−22.
(49) Zhang, H.; Lin, H.; Zheng, Y. Deactivation study of unsupported nano MoS_2 catalyst. *Carbon Resources Conversion* **2020**, *3*, 60−66.
(50) Travert, A.; Dujardin, C.; Maugé, F.; Cristol, S.; Paul, J. F.; Payen, E.; Bougeard, D. Parallel between infrared characterisation and ab initio calculations of CO adsorption on sulphided Mo catalysts. *Catal. Today* **2001**, *70* (1), 255−269.
(51) Dujardin, C.; Lélias, M. A.; van Gestel, J.; Travert, A.; Duchet, J. C.; Maugé, F. Towards the characterization of active phase of (Co)Mo sulfide catalysts under reaction conditions—Parallel between IR spectroscopy, HDS and HDN tests. *Applied Catalysis A: General* **2007**, *322*, 46−57.
(52) Schachtl, E.; Zhong, L.; Kondratieva, E.; Hein, J.; Gutiérrez, O. Y.; Jentys, A.; Lercher, J. A. Understanding Ni promotion of MoS_2/γ-Al_2O_3 and its implications for the hydrogenation of phenanthrene. *ChemCatChem.* **2015**, *7* (24), 4118−4130.
(53) Hadjiivanov, K.; Knözinger, H. FTIR study of the low-temperature adsorption and co-adsorption of CO and N_2 on NaY zeolite: evidence of simultaneous coordination of two molecules to one Na^+ site. *Chem. Phys. Lett.* **1999**, *303* (5−6), 513−520.
(54) Spatzal, T.; Perez, K. A.; Einsle, O.; Howard, J. B.; Rees, D. C. Ligand binding to the FeMo-cofactor: structures of CO-bound and reactivated nitrogenase. *Science* **2014**, *345* (6204), 1620−1623.
(55) Buscagan, T. M.; Perez, K. A.; Maggiolo, A. O.; Rees, D. C.; Spatzal, T. Structural characterization of two CO molecules bound to the nitrogenase active site. *Angew. Chem., Int. Ed.* **2021**, *133* (11), 5768−5771.

https://doi.org/10.1021/jacsau.1c00507
JACS Au 2022, 2, 613−622

(56) Travert, A.; Maugé, F. IR study of hydrotreating catalysts in working conditions: Comparison of the acidity present on the sulfided phase and on the alumina support. In *Studies in surface science and catalysis*; Delmon, B., Froment, G. F., Grange, P., Eds.; Elsevier: 1999; Vol. *127*, pp 269−277.
(57) Oliviero, L.; Vimont, A.; Lavalley, J.-C.; Sarria, F. R.; Gaillard, M.; Maugé, F. 2,6-Dimethylpyridine as a probe of the strength of Brønsted acid sites: study on zeolites. Application to alumina. *Phys. Chem. Chem. Phys.* **2005**, *7* (8), 1861−1869.
(58) Schachtl, E.; Kondratieva, E.; Gutiérrez, O. Y.; Lercher, J. A. Pathways for H_2 activation on (Ni)-MoS_2 catalysts. *J. Phys. Chem. Lett.* **2015**, *6* (15), 2929−2932.
(59) Lukoyanov, D. A.; Khadka, N.; Yang, Z.-Y.; Dean, D. R.; Seefeldt, L. C.; Hoffman, B. M. Hydride conformers of the nitrogenase FeMo-cofactor two-electron reduced state E_2(2H), assigned using cryogenic intra electron paramagnetic resonance cavity photolysis. *Inorg. Chem.* **2018**, *57* (12), 6847−6852.
(60) DuBois, M. R.; VanDerveer, M. C.; DuBois, D. L.; Haltiwanger, R. C.; Miller, W. K. Characterization of reactions of hydrogen with coordinated sulfido ligands. *J. Am. Chem. Soc.* **1980**, *102* (25), 7456−7461.
(61) Jones, L. O.; Mosquera, M. A.; Ratner, M. A.; Schatz, G. C. Control of charge carriers and band structure in 2D monolayer molybdenum disulfide via covalent functionalization. *ACS Appl. Mater. Interfaces* **2020**, *12* (4), 4607−4615.
(62) Byskov, L. S.; Nørskov, J. K.; Clausen, B. S.; Topsøe, H. DFT calculations of unpromoted and promoted MoS_2-based hydrodesulfurization catalysts. *J. Catal.* **1999**, *187* (1), 109−122.
(63) Singh, D. M. D. J.; Pradeep, T.; Bhattacharjee, J.; Waghmare, U. Novel cage clusters of MoS_2 in the gas phase. *J. Phys. Chem. A* **2005**, *109* (33), 7339−7342.
(64) Lacroix, M.; Jobic, H.; Dumonteil, C.; Afanasiev, P.; Breysse, M.; Kasztelan, S. Role of adsorbed hydrogen species on ruthenium and molybdenum sulfides. Characterization by inelastic neutron scattering, thermoanalysis methods and model reactions. In *Studies in Surface Science and Catalysis*; Hightower, J. W., Nicholas Delgass, W., Iglesia, E., Bell, A. T., Eds.; Elsevier: 1996; Vol. *101*, pp 117−126.
(65) Neese, F.; Wennmohs, F.; Becker, U.; Riplinger, C. The ORCA quantum chemistry program package. *J. Chem. Phys.* **2020**, *152* (22), 224108.
(66) Neese, F. Software update: the ORCA program system, version 4.0. *WIREs Computational Molecular Science* **2018**, *8* (1), e1327.
(67) Neese, F. The ORCA program system. *WIREs Computational Molecular Science* **2012**, *2* (1), 73−78.
(68) Grimme, S.; Ehrlich, S.; Goerigk, L. Effect of the damping function in dispersion corrected density functional theory. *J. Comput. Chem.* **2011**, *32* (7), 1456−1465.
(69) Grimme, S.; Antony, J.; Ehrlich, S.; Krieg, H. A consistent and accurate ab initio parametrization of density functional dispersion correction (DFT-D) for the 94 elements H-Pu. *J. Chem. Phys.* **2010**, *132* (15), 154104.
(70) van Wüllen, C. Molecular density functional calculations in the regular relativistic approximation: Method, application to coinage metal diatomics, hydrides, fluorides and chlorides, and comparison with first-order relativistic calculations. *J. Chem. Phys.* **1998**, *109* (2), 392−399.
(71) Weigend, F.; Ahlrichs, R. Balanced basis sets of split valence, triple zeta valence and quadruple zeta valence quality for H to Rn: Design and assessment of accuracy. *Phys. Chem. Chem. Phys.* **2005**, *7* (18), 3297−3305.
(72) Weigend, F. Accurate Coulomb-fitting basis sets for H to Rn. *Phys. Chem. Chem. Phys.* **2006**, *8* (9), 1057−1065.
(73) Pantazis, D. A.; Neese, F. All-electron scalar relativistic basis sets for the 6p elements. *Theor. Chem. Acc.* **2012**, *131* (11), 1−7.
(74) Pantazis, D. A.; Neese, F. All-electron scalar relativistic basis sets for the actinides. *J. Chem. Theory Comput.* **2011**, *7* (3), 677−684.
(75) Pantazis, D. A.; Neese, F. All-electron scalar relativistic basis sets for the lanthanides. *J. Chem. Theory Comput.* **2009**, *5* (9), 2229−2238.
(76) Pantazis, D. A.; Chen, X.-Y.; Landis, C. R.; Neese, F. All-electron scalar relativistic basis sets for third-row transition metal atoms. *J. Chem. Theory Comput.* **2008**, *4* (6), 908−919.
(77) Rolfes, J. D.; Neese, F.; Pantazis, D. A. All-electron scalar relativistic basis sets for the elements Rb-Xe. *J. Comput. Chem.* **2020**, *41* (20), 1842−1849.
(78) Petrenko, T.; Kossmann, S.; Neese, F. Efficient time-dependent density functional theory approximations for hybrid density functionals: Analytical gradients and parallelization. *J. Chem. Phys.* **2011**, *134* (5), 054116.
(79) Izsák, R.; Neese, F. An overlap fitted chain of spheres exchange method. *J. Chem. Phys.* **2011**, *135* (14), 144105.
(80) Neese, F.; Wennmohs, F.; Hansen, A.; Becker, U. Efficient, approximate and parallel Hartree-Fock and hybrid DFT calculations. A 'chain-of-spheres' algorithm for the Hartree-Fock exchange. *Chem. Phys.* **2009**, *356* (1−3), 98−109.

https://doi.org/10.1021/jacsau.1c00507
JACS Au 2022, 2, 613−622